Reconstruction of TOF Images from Undersampled *k*-Data Using SENSE, GRAPPA, CS, CS-SENSE, SPIRiT, and L1-SPIRiT

Jerome Yerly[1,2], Michel Louis Lauzon[2,3], and Richard Frayne[2,3]

[1]*Electrical and Computer Engineering, University of Calgary, Calgary, AB, Canada,* [2]*Seaman Family MR Research Centre, Foothills Medical Centre, Calgary, AB, Canada,* [3]*Departments of Radiology and Clinical Neurosciences, University of Calgary, Calgary, AB, Canada*

Introduction: Detecting pathologies in small intracranial arteries could potentially help in the diagnosis and treatment of cerebral small vessel diseases, such as lacunar stroke. However, visualizing small intracranial arteries using standard clinical 3-T MR scanners is challenging, as it requires acquiring high-resolution and high signal-to-noise ratio (SNR) MR angiography images, while maintaining reasonable acquisition time. Recent advances in image reconstruction from sparsely sampled *k*-space data, such as compressed sensing[1] (CS) and parallel MR imaging[2-5] (pMRI), provide potential solutions to enable acquisition of higher resolution MRA datasets without increasing the total acquisition time. In this study, we investigated and compared SENSE[2], GRAPPA[3], CS[1], SPIRiT[4], CS-SENSE[5], and L1-SPIRiT[4] reconstructions to accelerate time-of-flight (TOF) MR imaging. These techniques have different sampling requirements; therefore, we expect the sparse sampling methodology to be a function of the reconstruction technique. By tailoring the sampling strategy to the reconstruction method, we hypothesize that the optimum sampling/reconstruction combination will enable visualizing small intracranial vessels.

Methods: I. Data Acquisition: All imaging experiments were performed in a healthy volunteer using a 3-T MR scanner (Discovery 750; General Electric Healthcare, Waukesha, WI) and a 12-channel head coil. We used a clinical 3D TOF vascular sequence to acquire fully sampled *k*-data with TR = 25 ms, TE = 3.7 ms, flip angle of 15º, acquisition matrix size = 256 × 192 × 64, and FOV = 256 × 192 × 6.4 cm^3. The *k*-data were then transferred to a workstation for offline processing. II. Data Undersampling: We simulated 4-fold accelerated acquisitions by undersampling the phase encodes in the k_y-k_z plane of the fully sampled *k*-data. To satisfy the CS requirement of incoherent aliasing interference, we randomly selected the phase-encode locations based on a probability density function[1] (PDF). For the GRAPPA, SPIRiT, and L1-SPIRiT undersampling approaches, we fully sampled a region (24×24 pixels) at the origin of *k*-space and used it to calibrate the kernel weights. We applied the same sampling scheme for the SENSE approach and used the fully sampled central region to calculate the sensitivity maps. To satisfy the L1-SPIRiT requirements, we sampled the data using a Poisson-Disk distribution[6]. For the CS-SENSE approach, we simulated a 2× undersampled SENSE acquisition in the k_y direction, coupled with 2× undersampling of the k_y-k_z phase encode plane for CS (*i.e.*, total acceleration factor of 4). III. Data Reconstruction: We reconstructed each k_y-k_z slice using SENSE, GRAPPA, CS, SPIRiT, CS-SENSE, and L1-SPIRiT. For the CS reconstruction, we used both the wavelet transform and total variation as sparsifying domains and adjusted the regularization parameters accordingly through visual inspection of the reconstructed images. For the SENSE reconstruction, we calculated the sensitivity maps by first dividing the low-resolution coil images by a reference image obtained via the sum-of-squares of the low-resolution images, and then fitting a fourth-order polynomial to the data. We reconstructed the SENSE images with the conjugate gradient method. The SPIRiT and L1-SPIRiT reconstructions were performed as described by Lustig[4]. The CS-SENSE reconstruction was carried out sequentially[5], *i.e.*, we first reconstructed the aliased images using CS and then used SENSE to unfold the final composite image. IV. Reconstruction Assessment: We quantitatively assessed the reconstructed TOF source images by measuring the root-mean-square error (RMSE) at different locations between the accelerated images and the fully sampled reference image. The stacks of reconstructed images were also qualitatively assessed by visually comparing maximum intensity projections (MIP) of the whole data volumes. Close attention was paid to how well the small intracranial arteries were depicted in terms of conspicuity and feature detail.

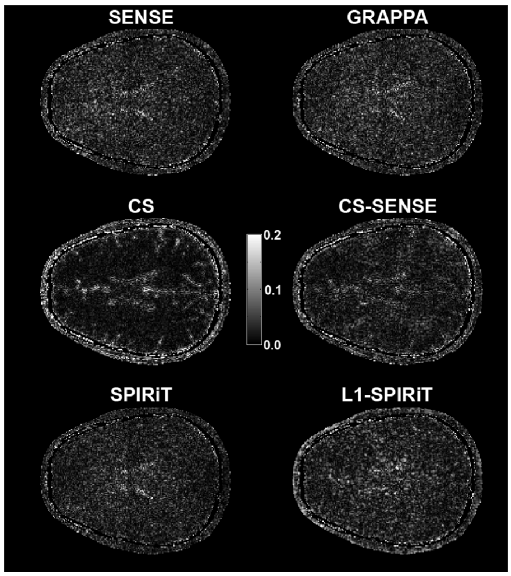

Figure 1: Maps of absolute normalized errors between a fully sampled TOF source image and the corresponding accelerated images.

Results: Figure 1 shows maps of absolute errors between a fully sampled TOF source image and the corresponding accelerated images. Overall, the CS reconstruction yielded less accurate images (highest RMSE values) than the other methods. CS performed particularly poorly in regions with sharp edges, *i.e.*, regions with high frequencies. However, it performed the best in homogeneous regions, *i.e.*, regions with low frequencies. The SENSE and CS-SENSE reconstructions performed better than CS in terms of RMSE, but they suffered from visible fold-over artifacts in the final composite images. The GRAPPA, SPIRiT, and L1-SPIRiT reconstructions provided similar results, however SPIRiT consistently yielded the lowest RMSE values. Figure 2a shows the MIP rendered image from the coronal view of the fully sampled TOF data. The arrows indicate the locations of two visible lenticulostriate arteries. Figure 2b shows an enlarged and rotated view of the lenticulostriate artery as given by the arrow with a star in Figure 2a. Figures 2c-2f show the enlarged views corresponding to the different accelerated reconstructions. Qualitative comparison of these MIP images reveals that the reconstructions involving an L1-norm regularization procedure (*i.e.*, CS, CS-SENSE, and L1-SPIRiT) resulted in lower aliasing interference, but also less conspicuous small intracranial vessels due to blurring. The SPIRiT and GRAPPA reconstructions best depicted the lenticulostriate arteries.

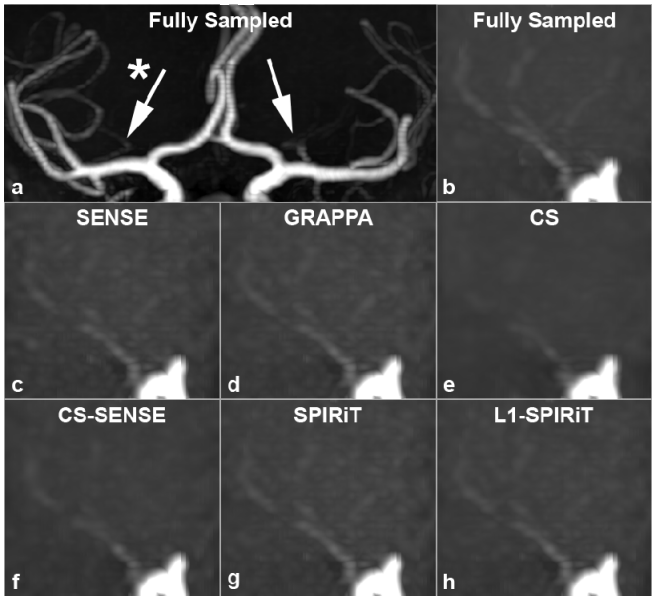

Figure 2: MIP rendered images: (a) coronal view of the fully sampled TOF data showing two lenticulostriate arteries, (b-h) enlarged and rotated views of the region as given by the arrow with a star corresponding to the different reconstructions. ***Acknowledgement:*** *David Gobbi for the MIP visualization software.*

Discussions: Although the CS reconstruction significantly reduced the background noise (*i.e.*, aliasing interference) in the MIP images, it could not depict the small arteries as reliably as the other approaches. A possible explanation is that forcing sparsity in the wavelet domain introduces some blurring in the reconstructed images. This blurring arises from the inherent property of the wavelet transform to concentrate most of the energy at the coarsest scale coefficients, which are closely related to the low frequencies of *k*-data. Thus, forcing sparsity in the wavelet domain tends to preserve coarse scale coefficients (corresponding to low frequencies) and discard detail scale coefficients (corresponding to high frequencies). The quality of the SENSE reconstruction highly depends on the accuracy of the sensitivity maps, and is thus vulnerable to magnetic field inhomogeneities/susceptibilities. In general, the SENSE reconstruction yielded accurate images. However, in slices with air-tissue interfaces, the difference of susceptibilities led to inaccurate sensitivity maps and resulted in significant fold-over artifacts in the final composite image. The auto-calibrating techniques, *i.e.*, GRAPPA, SPIRiT, and L1-SPIRiT, exhibited less sensitivity to susceptibilities artifacts and most reliably depicted the lenticulostriate arteries.

1. Lustig M, *et al. Magn Reson Med* 2007;58:1182. 2. Pruessmann KP, *et al. Magn Reson Med* 2001;46:638. 3. Griswold MA, *et al. Magn Reson Med* 2002;47:1202.
4. Lustig M, *et al. Magn Reson Med* 2010;64:457. 5. Liang D, *et al. Magn Reson Med* 2009;62:1574. 6. Dunbar D, *et al. ACM Trans Graph* 2006;25:503.